AD_____

Award Number: DAMD17-02-1-0112

TITLE: Corrective [111]In Capromab Pendetide SPECT Image Reconstruction Methods for Improved Detection of Recurrent Prostate Cancer

PRINCIPAL INVESTIGATOR: Benjamin M. W. Tsui, Ph.D.

CONTRACTING ORGANIZATION: Johns Hopkins University
                          Baltimore, MD 21205

REPORT DATE: June 2006

TYPE OF REPORT: Final

PREPARED FOR: U.S. Army Medical Research and Materiel Command
               Fort Detrick, Maryland 21702-5012

DISTRIBUTION STATEMENT: Approved for Public Release;
                        Distribution Unlimited

The views, opinions and/or findings contained in this report are those of the author(s) and should not be construed as an official Department of the Army position, policy or decision unless so designated by other documentation.

REPORT DOCUMENTATION PAGE

Form Approved
OMB No. 0704-0188

1. REPORT DATE	2. REPORT TYPE	3. DATES COVERED
01-06-2006	Final	1 Feb 2002 – 18 May 2006

4. TITLE AND SUBTITLE

Corrective ^{111}In Capromab Pendetide SPECT Image Reconstruction Methods for Improved Detection of Recurrent Prostate Cancer

5a. CONTRACT NUMBER

5b. GRANT NUMBER
DAMD17-02-1-0112

5c. PROGRAM ELEMENT NUMBER

6. AUTHOR(S)

Benjamin M. W. Tsui, Ph.D.

5d. PROJECT NUMBER

5e. TASK NUMBER

5f. WORK UNIT NUMBER

7. PERFORMING ORGANIZATION NAME(S) AND ADDRESS(ES)

Johns Hopkins University
Baltimore, MD 21205

8. PERFORMING ORGANIZATION REPORT NUMBER

9. SPONSORING / MONITORING AGENCY NAME(S) AND ADDRESS(ES)
U.S. Army Medical Research and Materiel Command
Fort Detrick, Maryland 21702-5012

10. SPONSOR/MONITOR'S ACRONYM(S)

11. SPONSOR/MONITOR'S REPORT NUMBER(S)

12. DISTRIBUTION / AVAILABILITY STATEMENT
Approved for Public Release; Distribution Unlimited

13. SUPPLEMENTARY NOTES
  Original contains colored plates: ALL DTIC reproductions will be in black and white.

14. ABSTRACT

It is generally recognized that 111In capromab pendetide (PS) scans are technically challenging to perform and interpret, particularly with regard to pelvic SPECT studies used to detect possible disease in the prostate fossa and pelvic lymph node (LN). The hypothesis of this proposal is that the superior spatial resolution, high image contrast, and much reduced image artifacts that result from the corrective SPECT image reconstruction methods would substantially aid in the detection and diagnosis of prostate cancer. To test our hypothesis, we propose five specific aims: (1) to develop simulation tools and methods that allow efficient generation of accurate 111In PS projection data from the human pelvic area, (2) to study the effects of 3D image degrading factors on 111In PS SPECT images, (3) to develop 3D corrective image reconstruction methods for 111In PS SPECT that provide much improved image quality and quantitative accuracy by incorporating models of the 3D image degrading factors, (4) to evaluate the 3D corrective image reconstruction methods for clinical 111In PS SPECT studies using simulated patient data, and Hotelling and human observer studies, and (5) to evaluate the clinical efficacy of the corrective image reconstruction methods as applied to 111In PS SPECT using patient data.

15. SUBJECT TERMS
Prostate cancer, SPECT imaging, Simulation study, ROC analysis, Clinical evaluation

16. SECURITY CLASSIFICATION OF:			18. NUMBER OF PAGES	19a. NAME OF RESPONSIBLE PERSON
a. REPORT	**b. ABSTRACT**	**c. THIS PAGE**		USAMRMC
U	U	U		**19b. TELEPHONE NUMBER** *(include area code)*

17. LIMITATION OF ABSTRACT: UU — NUMBER OF PAGES: 30

Table of Contents

INTRODUCTION

Prostate carcinoma, a leading cause for male cancer deaths, was estimated to result in 180,400 new cases and 31,900 deaths in the year 2000[1]. Earlier detection of prostate cancer has resulted from screening with serum prostate-specific antigen (PSA), with detection of disease when it is more localized[2]. In order to treat prostate cancer appropriately, it is essential to have accurate staging data. Clinicians try to determine tumor size and location, degree of periprostatic extension and whether bone and/or lymph node (LN) metastases are present. Imaging techniques routinely used for this purpose include transrectal ultrasound, pelvic CT and MRI, and radionuclide bone scanning. Despite these efforts, initial evaluation of pre-surgical patients leads to understaging in as high as 40 to 71% of patients[3]. Detection of LN metastases has been difficult, since LN involvement in prostate cancer is often associated with normal sized nodes. Since detection of LN disease with pelvic CT and MRI depends upon LN enlargement, neither of these modalities has been very successful in detecting the spread of prostate cancer to nodes (MRI slightly better than CT). Pooled data from four MRI series demonstrate an overall sensitivity of 42% and specificity of 98% [4].

Imaging with ^{111}In capromab pendetide (PS), a monoclonal antibody agent utilizing an indium-labeled antibody to prostate-specific membrane antigen (present in increased amounts in prostate cancer cells) has proven useful in detecting LN metastases. It is particularly useful in the detection of recurrent prostate carcinoma in patients who have had radical prostatectomy for their disease, but who have increasing PSA levels indicating the presence of an additional tumor. In a multi-institutional study, ^{111}In PS scanning localized disease in 108 of 181 patients (60%) with uptake in the prostatic fossa in 62 patients (34%), pelvic LN in 40 patients (22%) and abdominal LN in 42 patients (23%)[5]. Results were evaluated for the prostate fossa by ultrasound guided biopsy: 59 patients had positive biopsies for recurrent tumor, but only 29 of these had positive scans for a sensitivity of 49%[6]. The investigators felt that the false negative scans were likely to be due to small tumor volume. Results are more difficult to confirm for disease outside the prostatic fossa, since the LN metastases will usually be too small for detection by CT or MRI.

It is generally recognized that ^{111}In PS scans are technically challenging to perform and interpret[5], particularly with regard to the pelvic SPECT study used to detect possible disease in the prostate fossa and pelvic LN. Certainly part of this challenge is the detection of increased uptake in relatively small tumors in the pelvis.

In our preliminary study, we have demonstrated that corrective image reconstruction techniques that accurately correct for attenuation, collimator-detector response and scatter can significantly improve the quality and quantitative accuracy of ^{111}In PS SPECT images. The hypothesis of this proposal is that the superior spatial resolution, high image contrast, and much reduced image artifacts that result from the corrective SPECT image reconstruction methods would substantially aid in the detection and diagnosis of prostate cancer.

To test our hypothesis, we propose five specific aims: (1) to develop simulation tools and methods that allow efficient generation of accurate ^{111}In PS projection data from the human pelvic area, (2) to study the effects of 3D image degrading factors on ^{111}In PS SPECT images, (3) to develop 3D corrective image reconstruction methods for ^{111}In PS SPECT that provide much improved image quality and quantitative accuracy by incorporating models of the 3D image degrading factors, (4) to evaluate the 3D corrective image reconstruction methods for clinical ^{111}In PS SPECT studies using simulated populations of patient data, and Hotelling and human observer studies, and (5) to evaluate the clinical efficacy of the corrective image reconstruction methods as applied to ^{111}In PS SPECT using patient data.

BODY

As we discussed in our first and second year report, our entire laboratory relocated from the University of North Caroline at Chapel Hill (UNC-CH) to Johns Hopkins University (JHU) in July 1,

4

2002. We had an extremely smooth transition and were able to continue the research project with minimal interruption. In the following, we report of accomplishments addressing each of the proposed tasks.

Task 1.   *To develop simulation tools and methods for ^{111}In prostate SPECT (Months 1-18):*
        a.   Extend the realistic NCAT phantom to include the pelvic region of the body (Months 1-12)
        b.   Continue the development of a Monte Carlo simulation method that generates realistic projection data from the NCAT phantom with accurate models of the multiple photon emissions from ^{111}In, their attenuation and scatter in the body, and the geometric, penetration and scatter response of the collimator (Months 4-18)

Accomplishments:

We completed Task 1(a) in Year 1 as reported in the 1st year report and completed Task 1(b) in Year 2 as reported in the 1st year report. The following are extractions from the two previous reports.

A. We have completed Task 1a of the original proposal. The 3D NCAT (NRUB-based CArdiac Torso) phantom developed in our laboratory was extended for use in the project. Figure 1 shows the standard 3D NCAT phantom recently developed in our laboratory under the support of a separate NIH grant. Figure 2 shows the extension of the 3D NCAT phantom developed under the support of the present DOD research grant. Figure 3 shows the detailed anatomical structures including the prostate, bladder, key blood vessels and the 26 lymph nodes in the pelvic region of a male patient. Figure 4 shows sample slices through the phantom showing the simulated distribution of ^{111}In PS in the pelvic region that is based on clinical studies. Figure 5 shows the corresponding image slices showing the attenuation coefficient distribution.

B. We have made significant progress of Task 1b of the original proposal. We have successfully tested the MCNP Monte Carlo code that will be used in the research. Specifically, we implemented the extended 3D NCAT phantom in the MCNP code to generate list mode data of photons that were emitted from source distributions within the phantom, experienced photoelectric, scatter or no interaction with the tissue material of the phantom, and emerged from the surface of the phantom. In order to accurately simulate the response function of the medium collimator that are used in acquiring In-111 PS data, Monte Carlo simulation of photons through the collimator that include the effects of penetration and scatter within the collimator is desirable.   However, Monte Carlo simulation in both the phantom and collimator is extremely time-consuming even using the 90-node computer cluster in our laboratory.

C. Instead, we are developing a technique that pre-determine the collimator-detector response (CDR) function that includes the geometric, penetration and scatter components in a look-up table. The final projection data of the phantom will be obtained by reading the listmode data and run through the 3D CDR look-up table. The use of the look-up table provide a saving of computational time by a factor of over 100.
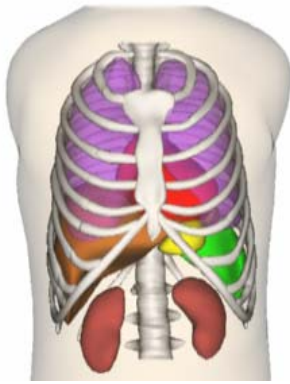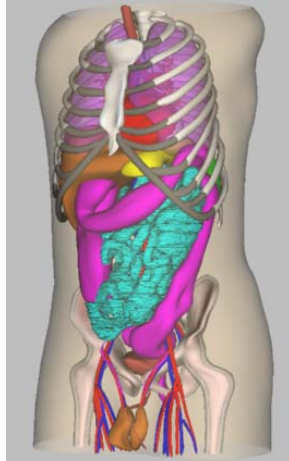
Figure 1. The standard 3D NCAT phantom

Figure 2. Extension of the 3D NCAT phantom to include the pelvic region.
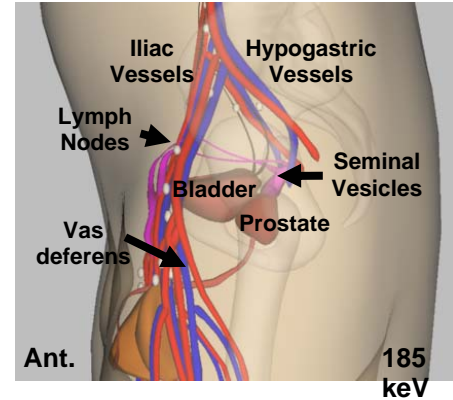

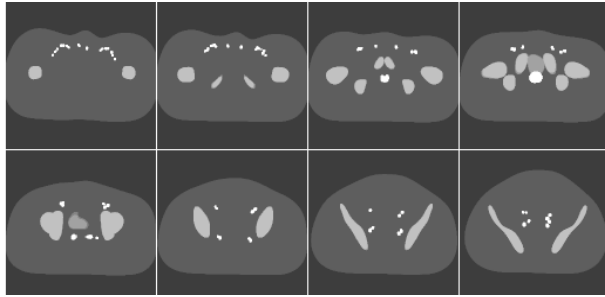Figure 3. Detail anatomical structures included in the extended NCAT phantom.

Figure 4. Sample slices through the pelvic region of the extended 3D NCAT phantom showing In-111 PS distribution. The slice thickness is 3.2 mm and the sample slices are selected every 8th slice from the complete set.
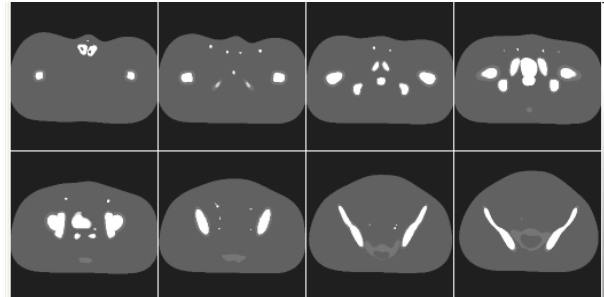

Figure 5. Corresponding slices through the extended 3D NCAT phantom as shown in Figure 4 showing the attenuation coefficient distribution.

D. In Year 2, we completed both parts (a) and (b) of Task 1. We determined the average uptakes of ^{111}In capromab pendetide (PS) in different organs based on the preliminary patient SPECT studies we acquired at UNC-CH before the present research grant started. The average uptakes in the different organs were used in the 3D NCAT phantom to develop an average ^{111}In PS radioactivity distribution phantom. A 3D attenuation distribution phantom was determined by assigning average attenuation coefficients for the ^{111}In photon energies to the bone structures and all tissues organs of the 3D NCAT phantom. Also, we identify the 26 possible sites of lymph nodes in the pelvic region. Figure 6 shows sample transaxial slices from the ^{111}In PS radioactivity distribution phantom with several of the lymph node sites. Figure 7 shows the corresponding transaxial slices from the attenuation distribution phantom.
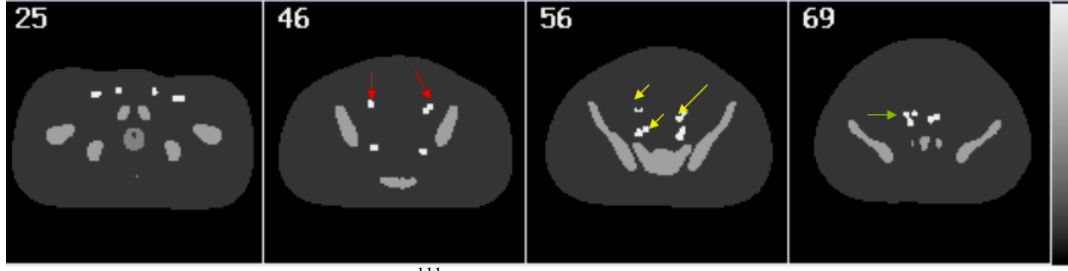
Figure 6. Sample transaxial slices of the ^{111}In PS radioactivity distribution phantom showing the prostate in the first slice, and with colored arrows pointing to several lymph nodes.
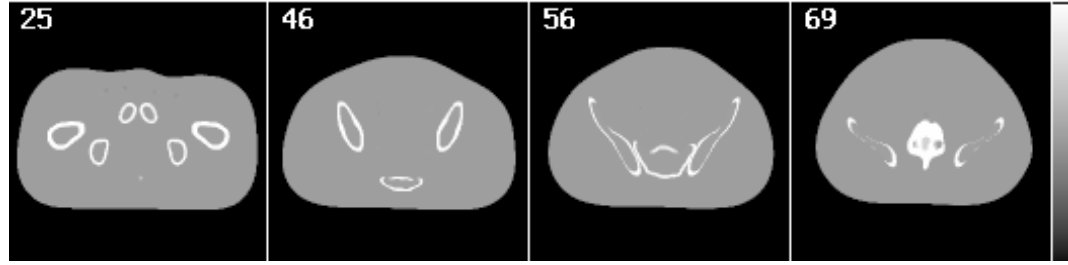

Figure 7. Sample transaxial slices from the attenuation distribution phantom.

E. Also in Year 2, we completed the development of a fast simulation method to generate projection data of the 3D ^{111}In PS phantom that accurate models the effects of photon attenuation and scatter within the phantom and the full collimator-detector response characteristics that include geometric, penetration and scatter components. The fast simulation method consists of two steps. In the first step, the SimSET Monte Carlo code developed at the University of Washington was used to simulate photon transport within the 3D phantom based on the ^{111}In PS uptake and attenuation distributions. The histories of photons exiting the phantom were saved in a history file for later use. In the second step, we apply a predetermined angular response function (ARF) specific for the collimator-detector used in the data acquisition and the ^{111}In photon energies to each photon in the photon history file. The ARF is the point source response function of the collimator-detector at the ^{111}In photon energies in angular increment. It is generated from the MCNP Monte Carlo code and includes the geometric, penetration and scatter components of the collimator-detector response.

F.   As shown in Figure 8, the predetermined ARF accurately models the collimator-detector response as compared to the results from Monte Carlo simulation using the MCNP code. Table 1 shows that the ARF method is 27 times faster than the MCNP Monte Carlo method in processomg 1 billion photon histories from the history file to simulate the image of an In-111 point source using a GE medium energy (ME) collimator. Since the ARF method is less susceptible to noise fluctuations due to the limited number of photon histories, there is an additional saving in processing time with the ARF method if the same image quality is used in the comparison. In the later case, the total saving in processing time with the ARF methods is 410 times that of the MCNP method. This is a critical development to allow us to perform the full simulation with a reasonable amount of computational time.
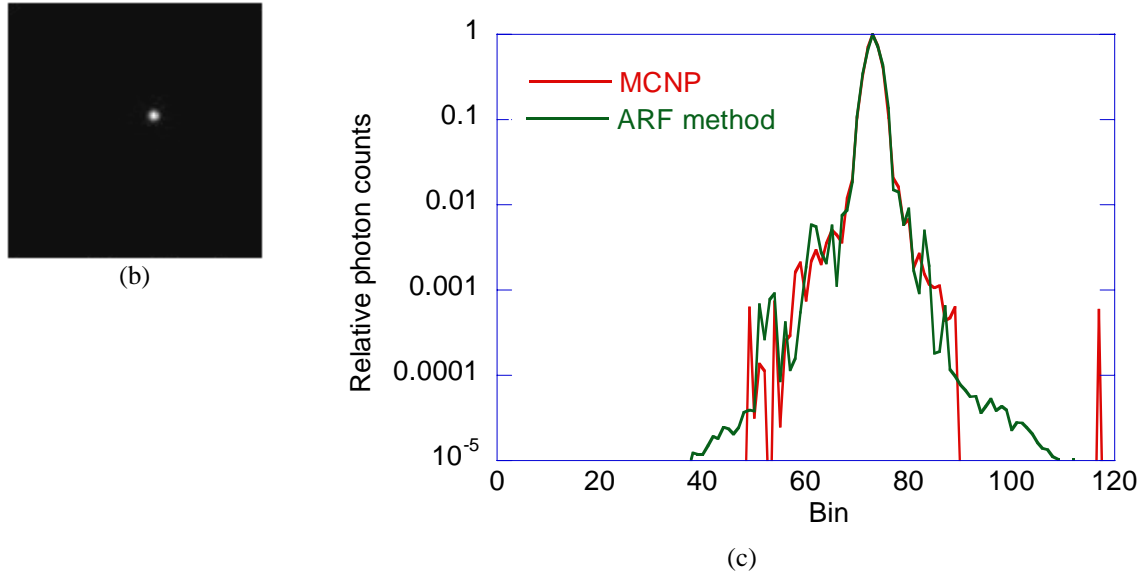

(a)

7

(b)

(c)
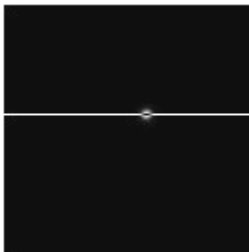
Figure 8. Projection images of an In-111 point source obtained using a GE medium energy (ME) collimator using (a) the MCNP Monte Carlo simulation code and (b) the fast ARF method. To obtain the same image quality, the number of the photons simulated using MCNP is 15 times that using the ARF. (c) Compareision of the horizontal profiles through the projection images.

Table 1. Comparison of the CPU times in simulating the collimator-detector response using the MCNP Monte Carlo code and the new ARF method

	Simulation Method	
	MCNP	**ARF**
Processing time to simulate 1 billion photon histories	2,873 sec	105 sec
Number of photon histories required to obtain the same image quality	15 billion	1 billion
Total CPU time	12 hours	105 sec

Figure 9 show sample projection images generated from the ^{111}In PS radioactivity and attenuation distributions generated from the 3D NCAT phantom using the fast simulation methods described above. They demonstrate the effectiveness of the simulation method to generate data that realistically mimic those acquired from an average patient.

Figure 9. Simulated projection data of the ^{111}In PS radioactivity and attenuation distribution phantoms, showing 6 views over a 360° range. As described in the text, they were generated using the SimSET Monte Carlo code to simulate photon transport through the phantom and the Angular Response Function (ARF) to simulate the full collimator-detector response characteristics. The data for each photopeak of ^{111}In were generated separately, and then summed.

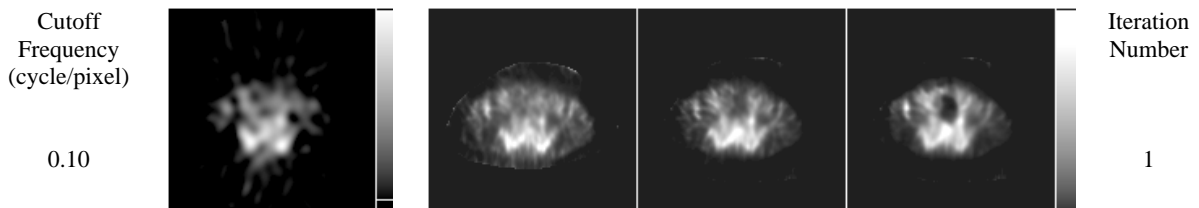*Task 2.* To study the effects of 3D image degrading factors on ^{111}In prostate SPECT (Months 4-21):
   a. Study the effect of photon attenuation in the patient's body on ^{111}In SPECT images (Months 4-12)
   b. Study the effects of photon scatter in patient's body on ^{111}In SPECT images (Months 7-15)
   c. Study the effects of collimator-detector response on ^{111}In SPECT images (Months 10-18)

Accomplishments:

We completed Task 2 (a), (b) and (c) in Year 1 and Year 2 as reported in the 1st and 2nd year report. The following are extractions from the 2 previous reports.

A. We have begun the study of the effects of 3D image degrading factors on ^{111}In prostate SPECT imaging in Year 1. As discussed in Task 3 below, we have developed and implemented corrective image reconstruction methods for ^{111}In prostate SPECT. The process allows us to study the effects of the degrading factor on the reconstructed images. For example, Figure 10 shows the reconstructed images from a patient study obtained using different corrective image reconstruction methods. Images on the left-most column were obtained from using the filtered backprojection (FBP) without any correction of the image degrading factors. Images on the right-most column were obtained using the OS-EM algorithm with correction of the CDR, attenuation and scatter in the patient. The result is closest to the true ^{111}In PS distribution. Images on the column second to the right-most column were obtained using the OS-EM algorithm with correction of the CDR and attenuation in the patient. They indicate the effect of scatter alone on the reconstructed images. Images on the column third to the right-most column were obtained using the OS-EM algorithm with correction of the CDR alone. They demonstrate the combined effects of attenuation and scatter in the patients on the reconstructed images.

Since we do not know the truth distribution in a patient study, the best method to study the effects of the image degrading factors is through simulation study. We are in the process of applying the extended 3D NCAT phantom and the simulation tools developed in Task 1 to study the effects of the degrading factors in more detail.

Cutoff
Frequency
(cycle/pixel)

0.10

Iteration
Number

1

9

	3D FBP	OS-EM	OS-EM	OS-EM	
0.15					2
0.20					5

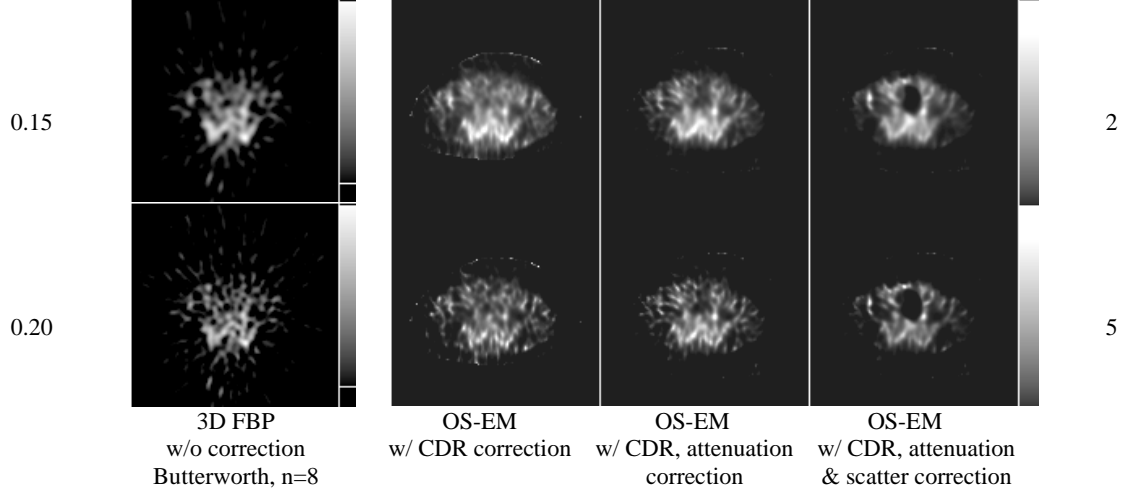| 3D FBP	OS-EM	OS-EM	OS-EM
w/o correction	w/ CDR correction	w/ CDR, attenuation	w/ CDR, attenuation
Butterworth, n=8		correction	& scatter correction

Figure 10. Reconstructed images from a patient study obtained using different corrective image reconstruction methods. *Left-Most Column:* Images were obtained from using the filtered backprojection (FBP) without any correction of the image degrading factors. *Second Column from the Left:* Images obtained using the OS-EM algorithm with correction of the CDR alone. *Third Column from the Left:* Images obtained using the OS-EM algorithm with correction of the CDR and attenuation in the patient. *Right-Most Column:* Images obtained using the OS-EM algorithm with correction of the CDR, and attenuation and scatter in the patient.

B. As shown in Figure 11, in Year 2 we have developed a fast Monte Carlo method that allows us to generate projection data that accurately model the effects of photon attenuation and scatter within the phantom and the full characteristics of the collimator-detector used. This is a very complicated process. The successful implementation of this fast Monte Carlo simulation capability also allows us to generate projection datasets that selectively include the effects of photon attenuation and/or scatter and/or characteristics of the collimator-detector used in the data acquisition. These datasets can be generated with much faster speed than those that include all the physical instrumentation effects.

C. The datasets that include the selected physical and instrumentation effects are reconstructed, organized and studied. The reconstructed images allow us to study the effects of photon attenuation and scatter in the patient's body and of the collimator-detector response characteristics on the ^{111}In SPECT images. Figure 5 shows an example of reconstructed images from the simulation study where the projection data were generated using the simulation method described above and include the effects of photon attenuation and scatter in the patient and the full imaging characteristics of the collimator-detector system. No compensation was used in the conventional filtered backpronection (FBP) reconstruction algorithm and the iterative OS-EM algorithm. The reconstruction images demonstrate the effects of photon attenuation and scatter and the collimator-detector response. Also, they demonstrate the iterative OS-EM reconstruction algorithm without compensation give similar reconstructed image artifacts as the conventional FBP algorithm.
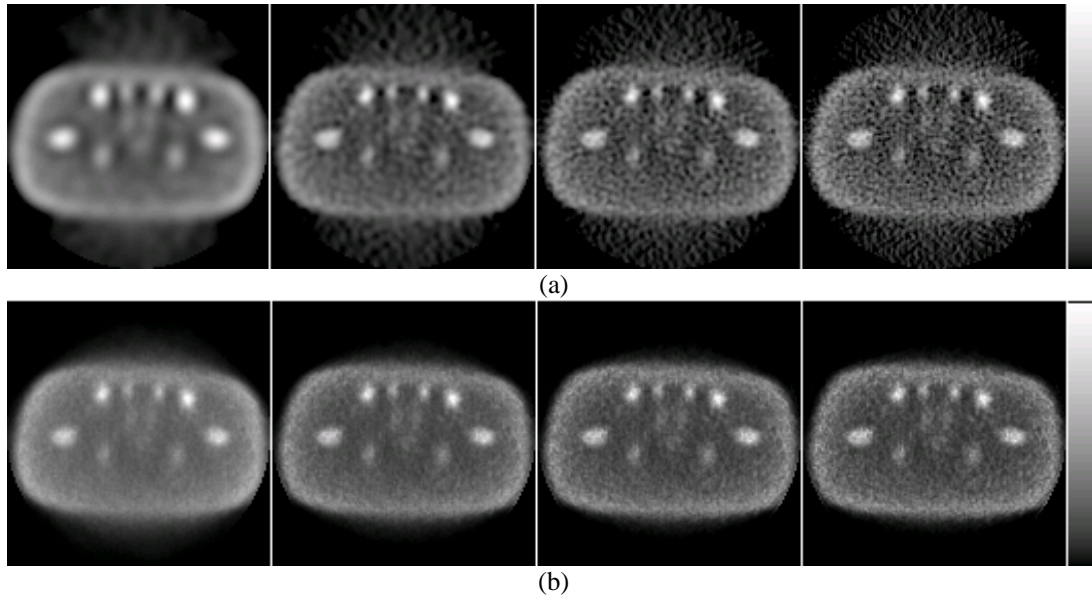
(a)

(b)

Figure 11. (a) Transaxial reconstructed images from a sample slice through the 3D NCAT phantom obtained using the filtered backprojection algorithm without any compensation. The images were post-filtered using a Butterworth filter with order 8 and, from left to right, filter cutoffs of 0.10, 0.20, 0.30 and 0.40 cycles/pixel, respectively. (b) Transaxial reconstructed images from the sample slice obtained using the iterative OS-EM algorithm without any compensation at, from left to right, the 1st, 2nd, 3rd and 4th iteration, respectively. Twelve subsets were used in the OS-EM algorithm.

Task 3. *To continue the development of 3D corrective image reconstruction methods for ^{111}In prostate SPECT that provide much improved images quality and quantitative accuracy by incorporating models of the 3D image degrading factors (Months 7-24):*
  a. *To use results from Task 2 to guide the development of methods to incorporate accurate models of image degrading factors in iterative and non-iterative 3D image reconstruction (Months 7-24)*

Accomplishments:

We completed Task 3 (a) in Year 1 and Year 2 as reported in the 1st and 2nd year report. The following are extractions from the previous two reports.

A. We have made significant progress in accomplishing Task 3a in Year 1 of the project. The corrective image reconstruction methods that are under development are based on iterative image reconstruction algorithms. As shown in Figure 12, a typical iterative reconstruction algorithm allows one to incorporate models of the imaging process in the projection and backprojection steps. Through the iterative process, accurate compensation of the effects of imaging degrading factors can be achieved.

B. We completed the implementation of accurate models of the collimator-detector response (CDR), and attenuation and scatter in the iterative ordered-subset expectation-maximization (OS-EM) image reconstruction algorithm to correct for their effects. Figure 13 shows the different components of CDR found in medium- and high-energy collimators at different energies. Typical experimental measured point response functions from these collimators are shown in Figure 14. We incorporate accurate model of the CDR of the collimator as a

function of source distances in the OS-EM algorithm as shown in Figure 12. To compensation for photon attenuation, we incorporate the attenuation distribution of the patient obtained from transmission CT studies. For scatter compensation, we apply the effective scatter source method as shown in Figure 15 developed in our laboratory.

C. Figure 10 shows preliminary results from applying the corrective image reconstruction to a clinical ^{111}In PS prostate SPECT study. They indicate the substantial improvement in image quality using the corrective image reconstruction methods especially when all the image degrading factors, i.e., CDR, and attenuation and scatter in the patient, are included in the correction.
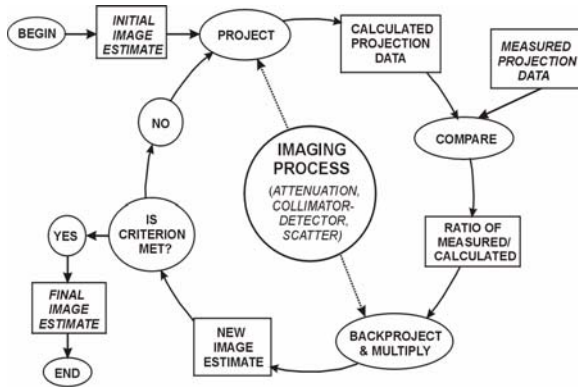

Figure 12. Corrective image reconstruction using iterative image reconstruction algorithms. Accurate models of the imaging process including the collimator-detector response (CDR) and attenuation and scatter in the patient can be incorporated in the iterative reconstruction algorithm to compensate for their effects.
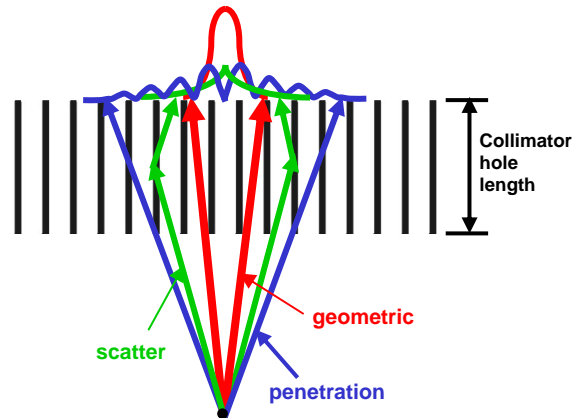

Figure 13. Components of collimator-detector response (CDR). For ME and HE collimator using ME and HE collimators, the penetration and scatter components are significant as compared to the geometric component.
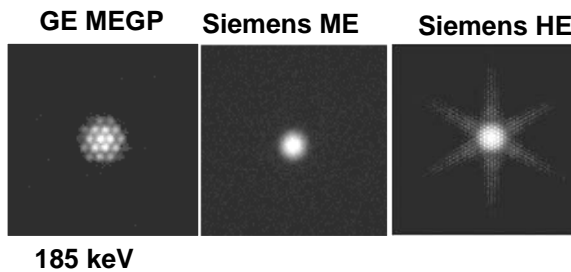

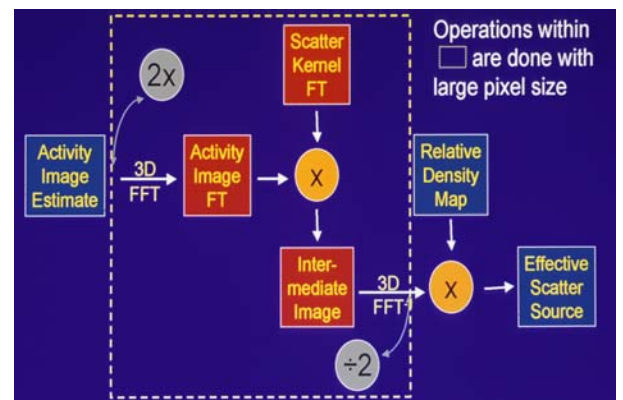Figure 14. Measured point response function of different medium- and high-energy collimators

Figure 15. Scatter correction methods based on effective scatter source that can be implemented in iterative image reconstruction methods.

D. We have accomplished the development of 3D corrective image reconstruction methods for ^{111}In prostate SPECT that provide much improved image quality and quantitative accuracy by incorporating models of the 3D image degrading factors. The 3D corrective image reconstruction methods incorporate accurate compensation of photon attenuation and scatter in the patient and the full characteristics of the collimator-detector response in the iterative OS-EM algorithm. The compensation methods utilize the results from Task 2 to guide the development

E. In Figure 16, we show the improvements in reconstructed image quality as the image corrective image reconstruction method incorporates different individual and combination of image degrading effects including photon attenuation and scatter in the patient and the full image characteristics of the collimator-detector response. Here results from a sample slice through the 3D NCAT phantom and noise-free simulated projection data as described in Task 2 were used.

F. In Figure 17, results from simulated noisy projection data from four sample slices through the 3D NCAT phantom and at three noise levels were shown. They demonstrate the ability of the corrective image reconstruction methods in processing realistic data as compared with the conventional FBP image reconstruction method without any compensation.
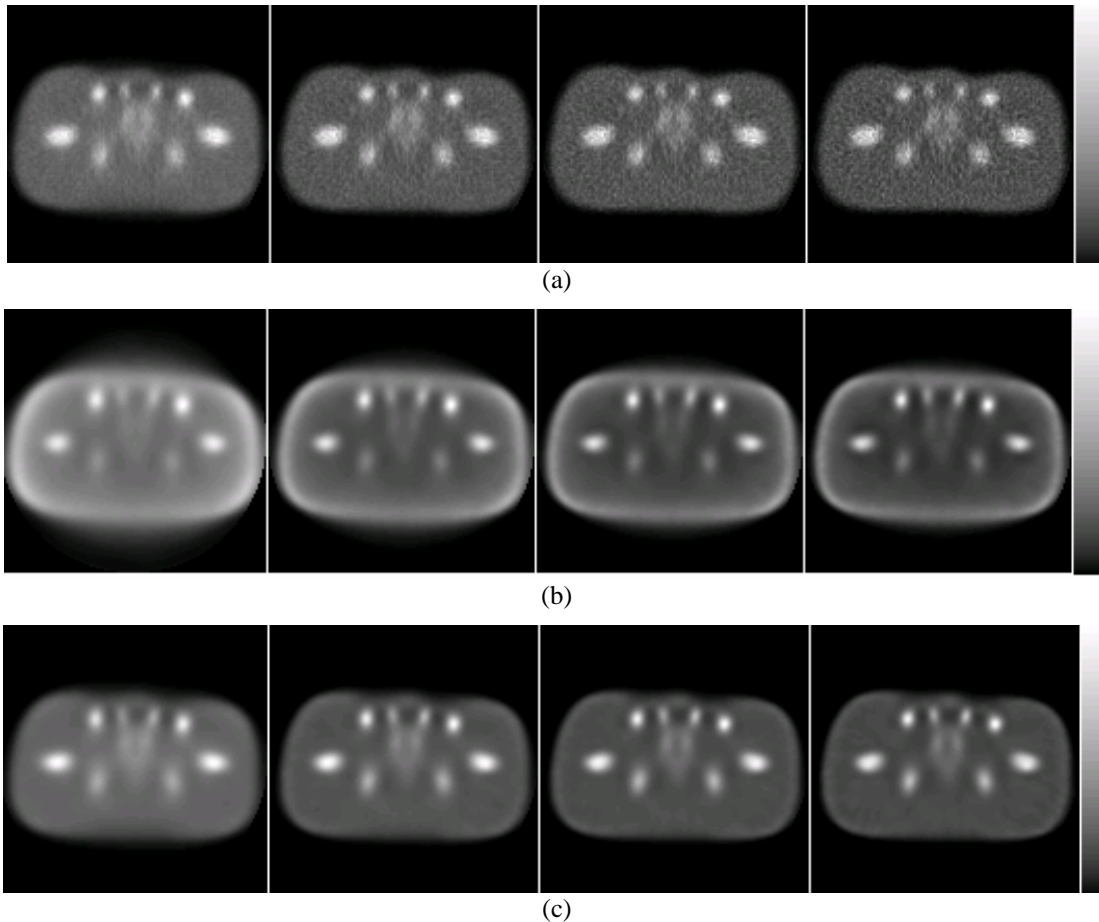

(a)

(b)

(c)

Figure 16. Transaxial reconstructed images of a sample slice through the 3D NCAT phantom using simulated noise-free projection data and corrective reconstruction method with compensation of individual and combination of image degrading effects. (a) Reconstructed images obtained using the iterative OS-EM algorithm with compensation of photon attenuation alone at, from left to right, 1st, 2nd, 3rd, and 4th iterations, respectively. (b) Reconstructed images obtained using the iterative OS-EM algorithm with compensation of the full collimator-detector response alone at, from left to right, 1st, 2nd, 3rd, and 4th iterations, respectively. (c) Reconstructed images

obtained using the iterative OS-EM algorithm with compensation of both photon attenuation and full collimator-detector response at, from left to right, 1st, 2nd, 3rd, and 4th iterations, respectively. Twelve subsets were used in the OS-EM algorithm.
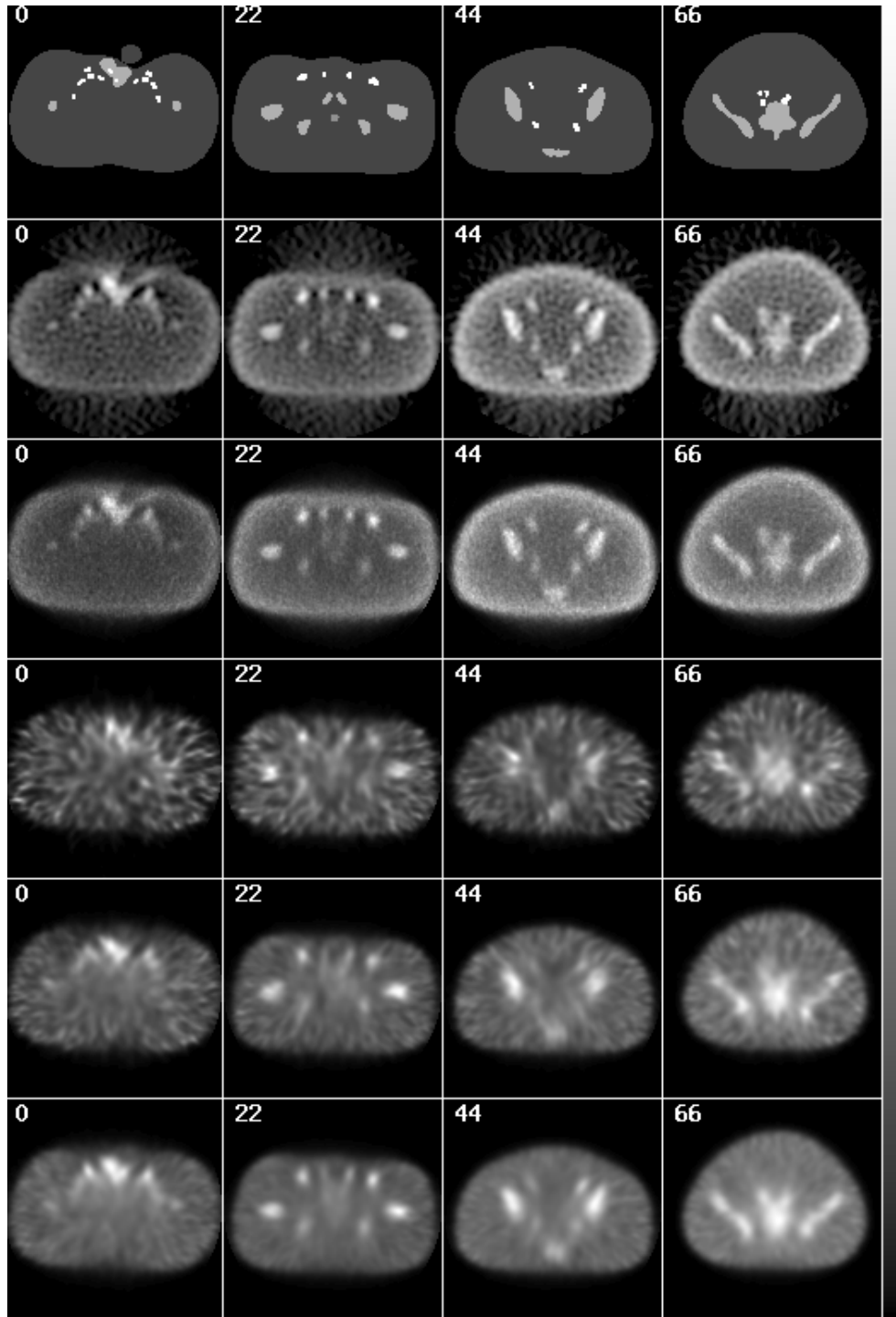
Figure 17. Results from simulation study to evaluate the effectiveness of the corrective image reconstruction method in improving the quality and quantitative accuracy of ^{111}In PS SPECT images. The four columns represent results from four different slices through the 3D NCAT phantom. *First Row:* The activity distribution of the image slices. *Second Row:* Transaxial reconstructed images obtained using the FBP algorithm and a Butterworth post-filter

with order 8 and cut-off frequency at 0.2 cycles/pixel. *Third Row:* Transaxial reconstructed images obtained using the iterative OS-EM algorithm with no compensation. *Fourth Row:* Transaxial reconstructed images obtained using the iterative OS-EM with compensation for attenuation and the full CDR, applied to noisy projection data with 5,000 counts/slice. *Fifth Row:* Similar to the fourth row except with 20,000 counts/slice. *Sixth Row:* Similar to the fourth row except with 80,000 counts/slice. Six subsets were used in the OS-EM algorithm.

Task 4. To evaluate the 3D corrective image reconstruction methods for [111]*In prostate SPECT using simulated populations of patient data, and Hotelling and human observers (Month 13-36):*
   a. *Evaluate the 3D corrective imaging reconstruction methods as applied to* [111]*In prostate SPECT using Hotelling observers and ROC analysis methods (Months 13-36)*
   b. *Evaluate the 3D corrective imaging reconstruction methods as applied to* [111]*In prostate SPECT using human observers and ROC analysis methods (Month 19-36)*

Accomplishments:

   We have made significant progress in the completing Task 4 in Year 3. We continue to made progress in the research in the form of presenting and submitting the results for presentations at national and international conferences and in publications as indicated by the record of presentations and publications.

A. As indicated in the Year 2 report, we began simulating data required for the evaluation study and made significant progress. In Year 3, we have continued the effort and have been working on the full scale data simulation for the Hotelling and human observer studies. Specifically, we have created a 'population' of phantoms that includes variations in patient anatomical structures as shown in Figure 18. The population consists of phantom with 3 body sizes, i.e., small, average and large, each with three different bone structure, i.e., small, medium and large. Also, to more realistically simulate patient data, we include possible air pockets in the intestines as shown in Figure 19.
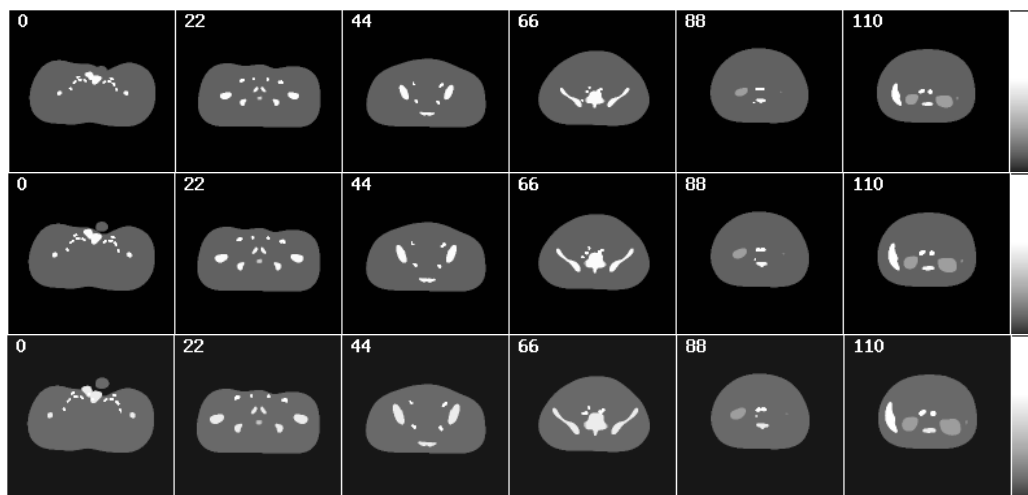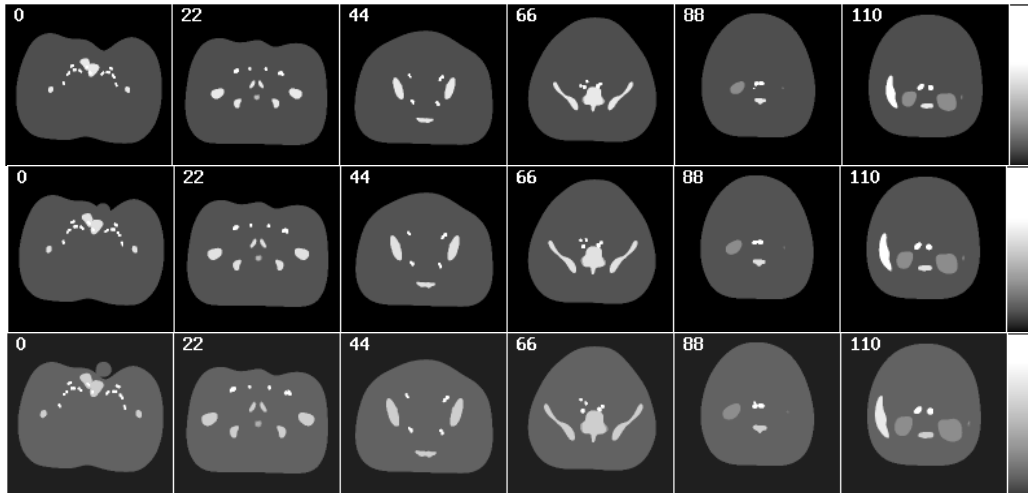

(a)
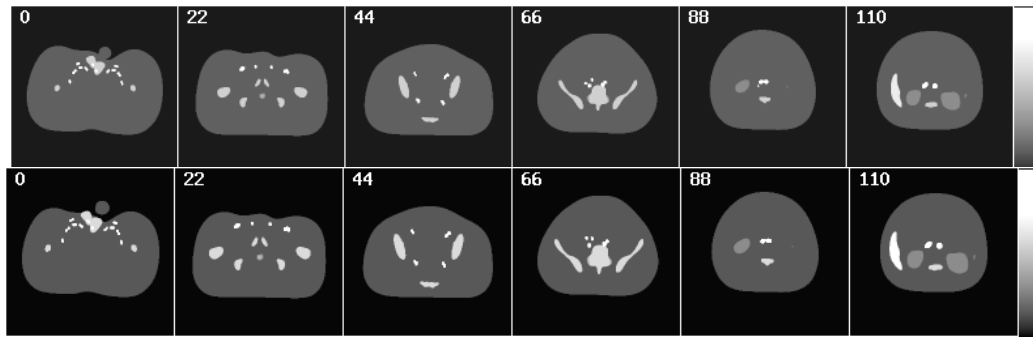
(b)

(c)

Figure 18. Family of 3D NCAT phantoms to be used in evaluation study with (a) small body size, (b) average body size, and (c) large body size. For each body size, (Top Row) small bone structure, (Middle Row) medium bone structure, and (Bottom Row) large bone structure.
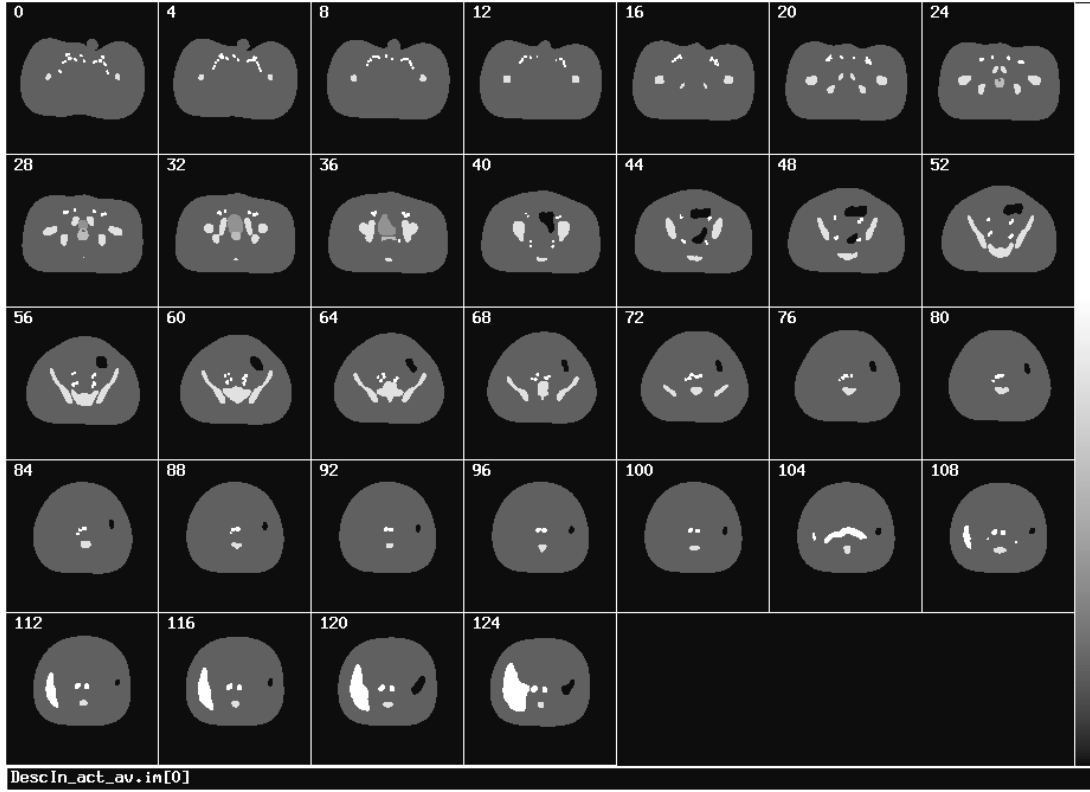
Figure 19. A 3D NCAT phantom that consists of air pockets in the intestines (the activity concentration is set to zero for easier visualization here; it is ~1:4 with respect to background in actual simulation). It demonstrates our ability to simulation the special anatomy found in some patient studies.

B. We have carefully checked the quantitative SPECT image reconstruction methods developed in this research grant and applied them to the Monte Carlo simulated projection data from the 3D NCAT phantom described earlier. Figure 20 shows sample results from the Monte Carlo simulation study. The top two rows show sample slices through the 3D NCAT phantom showing the radioactivity and attenuation coefficient distribution of the phantom. The SimSET Monte Carlo code was used to generate 'almost' noise-free projection data from the 3D NCAT phantom. The noise-free projection data were scaled to specific mean counts and Poisson noise fluctuations were then added to simulate the acquired projection data. Finally, the quantitative SPECT image reconstruction methods were applied to obtain the reconstructed images at different iteration number. The simulation study allows comparison of the reconstructed images with the phantom slices and demonstrate the quality and quantitative accuracy of the quantitative SPECT image reconstruction methods.
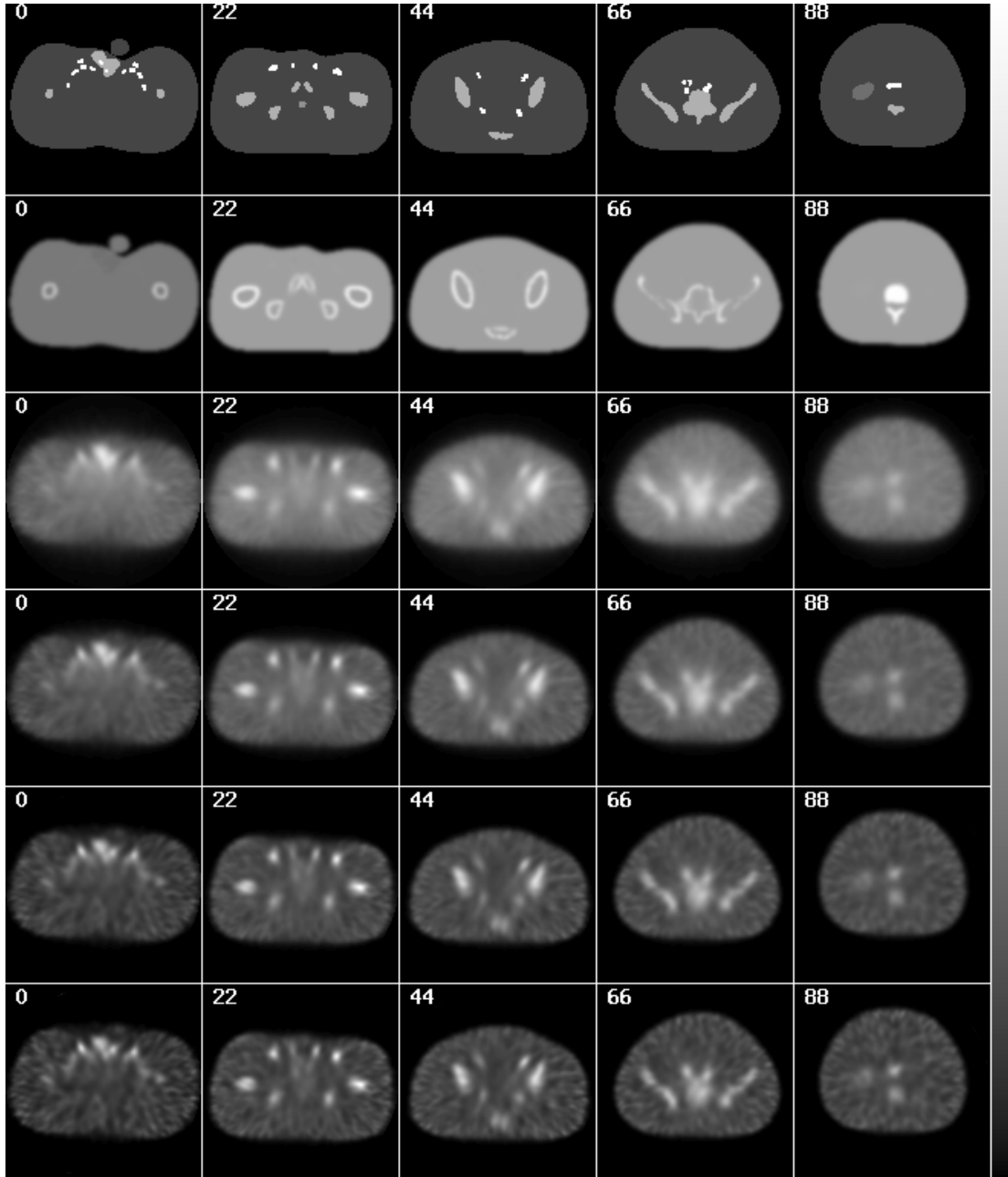
Figure 20. Sample reconstructed images obtained from applying the quantitative SPECT image reconstruction methods to the Monte Carlo simulated noisy projection data. *First Row:* Sample transaxial slices of the 3D NCAT phantom showing the radioactivity distribution. *Second Row:* Corresponding transaxial slices showing the attenuation coefficient distribution. Monte Carlo simulation method was used to generate 'almost' noise-fee projection data that include the effects of attenuation, scatter and collimator-detector response of a medium-energy collimator. They were then scaled to a total projection count of 80K and Poisson noise fluctuations were added to simulate the actual acquired data. The quantitative SPECT image reconstruction methods, based on the iterative OS-EM algorithm with 6 subsets, 20 angular projections per subset and correction of attenuation and the collimator-detector response after *Third Row:* 1 iteration, *Fourth Row:* 2 iteration, *Fourth Row:* 2 iteration, *Fifth Row:* 4 iteration, and *Sixth Row:* 6 iterations.

C. We have made plan for the Hotelling observer study to evaluate the efficacy of the quantitative SPECT image reconstruction methods as applied to ^{111}In labeled ProstaScint® SPECT images. The

null hypothesis is that there is no difference in lesion detectability (AUC) between the different reconstruction algorithms, i.e., filtered backprojection (FBP) with post-filtering using a Butterworth filter, the ordered-subsets expectation-maximization (OS-EM) algorithm with attenuation compensation (OSA), and OS-EM with attenuation and detector response compensation (OSAD).

To test this hypothesis, we propose to perform channelized Hotelling observer (CHO) study using simulated ProstaScint® data from a population of phantoms. The study consists of the following components.

a. Create a population of phantoms as described in Accomplishment #1. The population of phantoms consists of anatomical variations.
b. Vary the organ radionuclide uptake distribution (by randomly sampling from a distribution of uptake ratios) between phantoms, lesion size and location (3 different sizes & locations) and noise level, to mimic the variations seen in a human population.
c. Simulate projection data from the phantom population so as to obtain two classes of images – lesion-present (LP) and lesion-absent (LA) – for use in the CHO study.
d. Train the CHO with a training image set before applying it to test images.

The CHO study consists of the following sub-studies. These sub-studies are designed to determine the optimal image reconstruction parameters. The final result, that is, the best image reconstruction method will be derived from results of the sub-studies.
- To determine the optimal cut-off frequency for the Butterworth filter used in post-filtering of the FBP algorithm,
- To determine the optimal combination of iteration number and cut-off frequency for the Butterworth filter used in post-filtering of the OSA algorithm.
- To determine the optimal combination of iteration number and cut-off frequency for the Butterworth filter used in post-filtering of the OSAD algorithm.
The best image reconstruction method is the one that provides the highest lesion detectability, or largest area under the ROC curve, from the CHO studies.

The following list the details of the research plan. We have generated the projection data and reconstruction images for the study.

a. Number of phantoms: (18 from the following, i.e., 3x3x2)
    - 3 body sizes: small, average, large
    - 3 body frames for each body size: small, medium, large
    - 2 intestinal states: air in ascending portion of large intestine, air pockets in descending portion, air in sigmoidal colon & rectum.

b. Possible lymph node lesion locations: (3 as shown below and Figure 21)
    - Lesion in obturator node on the left side (slice 27)
    - Lesion in external iliac node on the right side (slice 45)
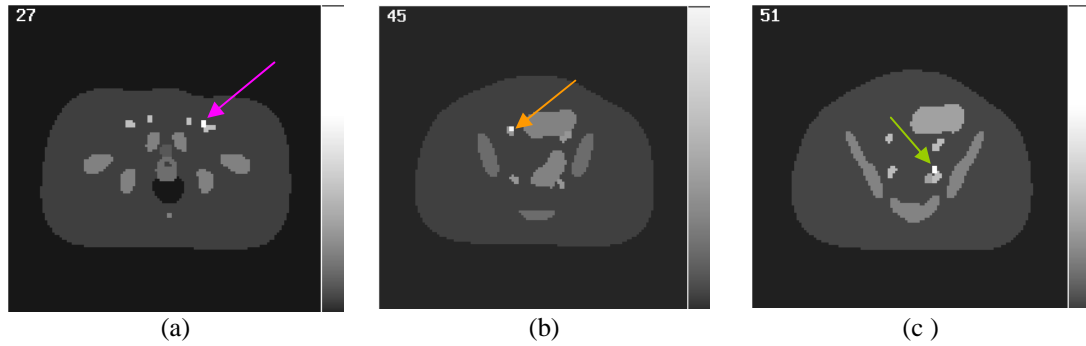   - Lesion in common iliac node on the left side (slice 51)

Figure 21. Possible lymph node lesion locations. (a) Lesion in obturator node on the left side (slice 27), (b) Lesion in external iliac node on the right side (slice 45), and Lesion in common iliac node on the left side (slice 51).

c. Noise levels: (3 levels) at 7,000, 14,000 and 28,000 counts per slice

d. Total number of images that will be generated: (Total of 324 LP and LA images)
    - Lesion present (LP): 18 phantoms x 3 lesions x 3 noise levels = 162 images; half of these (81) will be the LP images used for the training of the CHO, and the other half (81) will be used for testing.
    - Lesion absent (LA): 18 phantoms x 3 sets of noise realization (varied uptake ratios) x 3 noise levels = 162 images; half of these LA images will be used in training of the CHO, and the other half (81) will be used for testing.

e. Total number of ROC curves that will be generated: (Total of 55 ROC curves)
    - Filtered Backprojection (FBP) with the Butterworth filter:
        5 filter cutoffs = 5 curves
    - OS-EM with attenuation correction (OSA) and Butterworth post-filtering:
        5 updates x 5 post-reconstruction filter cutoffs = 25 curves
    - OS-EM with attenuation and detector response correction (OSAD) and Butterworth postfiltering:
        5 updates x 5 post-reconstruction filter cutoffs = 25 curves
    - Total number of ROC curves that will be generated from this CHO study
        5 (FBP) + 25 (OS-A) + 25 (OS-AD) = 55

f. Preliminary CHO study results
        Figur 22 show preliminary result of the CHO studies. They are obtained with a small test image set resulting in a fairly large error bars. However, despite the relatively large error bars, the preliminary results indicate clearly the superior image quality in terms of detection of small lesions for the ^{111}In PS SPECT images obtained with the quantitative SPECT image reconstruction methods as compared to the FBP algorithm without any correction. These preliminary results also demonstrate that all the components of the simulation study are working properly. Based on results of the preliminary study, we are proceeding onto the full scale simulation study using the CHO to evaluate the quantitative image reconstruction methods for prostate SPECT.
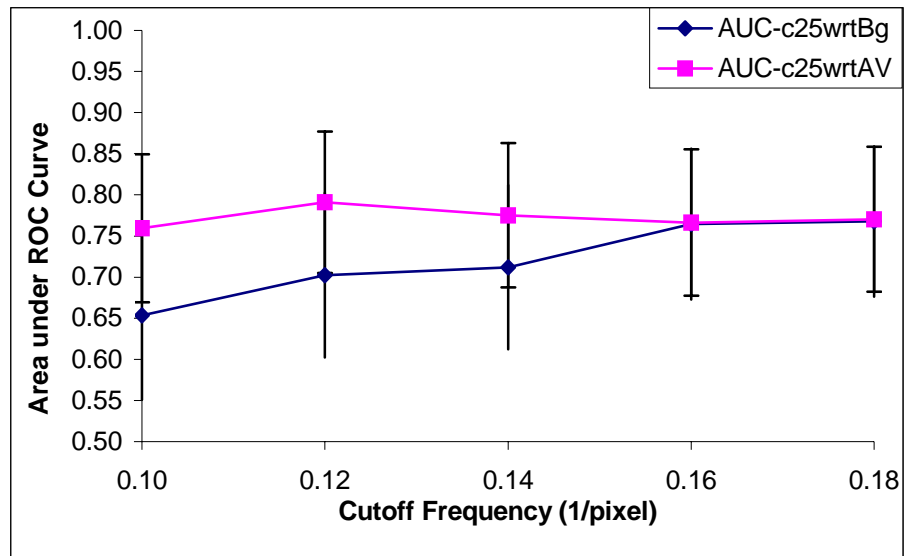
(a)
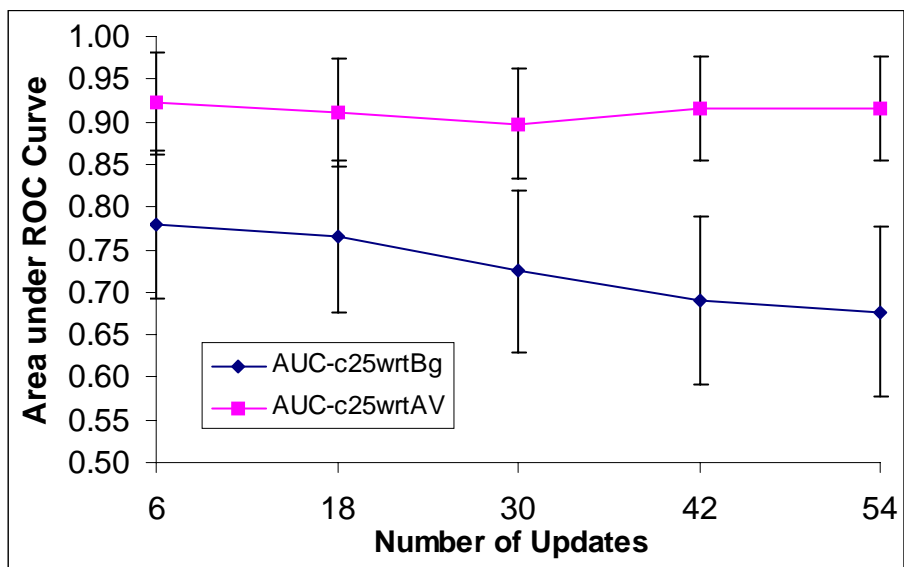
(b)
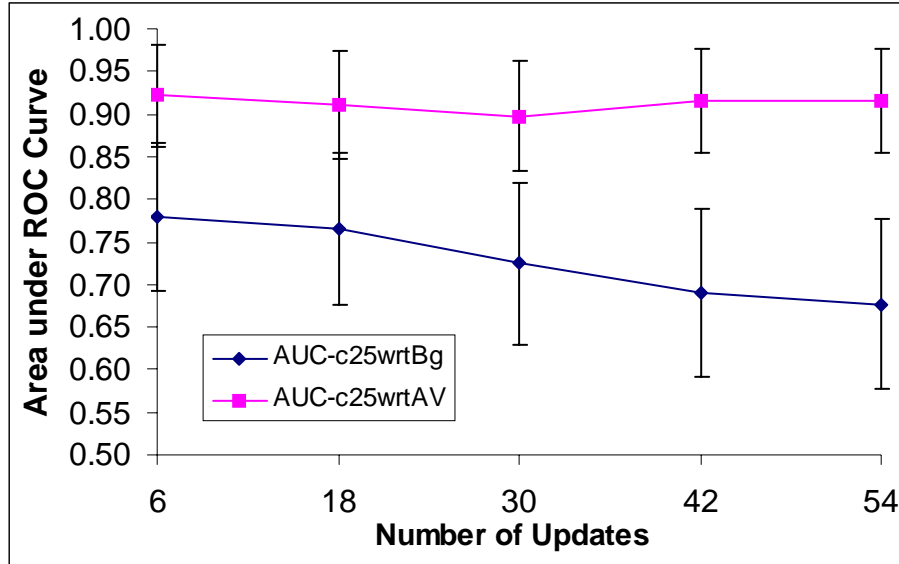
(c)

*Figure 22. The areas under the ROC curve from the preliminary CHO study (a) as a function of cutoff frequency using the FBP algorithm without correction, (b) as a function of number of updates (number of subsets * number of iterations) using the iterative OS-EM reconstruction algorithm, with compensation for attenuation (OSA), and (c) as a function of number of updates (number of subsets * number of iterations) using the iterative OS-EM reconstruction algorithm, with compensation for attenuation and detector response (OSAD). The results in pink are from 25% lesion contrast with respect to background and the results in blue are with respect to the arteries & veins.*

<u>*Task 5.*</u> *To evaluate the clinical efficacy of the corrective image reconstruction methods using patient ^{111}In prostate SPECT data (Month 1-36):*
   a. *To set up the GE VG/Hawkeye dual-head SPECT system for ^{111}In PS SPECT data acquisition from patients (Month 1-3)*
   b. *To acquire ^{111}In PS SPECT data acquisition from patients (Month 4-33)*
   c. *To process the patient ^{111}In PS SPECT data using the corrective image reconstruction methods developed in Task 3 (Month 4-33)*
   d. *To conduct clinical evaluation of the patient ^{111}In PS SPECT data (Month 13-33)*
   e. *Statistical analysis of evaluation data (Month 31-36)*

Accomplishments:

A. Task 5 (a) has been completed in Year 1.

B. In regard to Task 5 (b), we have obtained IRB approval since our laboratory relocated to Johns Hopkins University (JHU). During Year 2, we have worked with the nuclear medicine clinic at JHU to modify the ^{111}In PS SPECT data acquisition protocol to improve the quality of the acquired data. There is a slight delay in the clinical data acquisition due to the relocation and the application of the IRB. However, the official patient data acquisition and processing has begun. As of April 2006, we have acquired data from 21 patient studies, i.e., 15 new cases during that last 12 months. Figure 8 shows results from one of the patient datasets.

C. We are in the process of checking the clinical data and applying the different image reconstruction methods.

D. Also, we are planning on the clinical evaluation study using the clinical data and the patient record for the 'truth' state of the patients.

E. Figure 22 show a typical set of for ^{111}In PS SPECT/CT images obtained from the patient study.
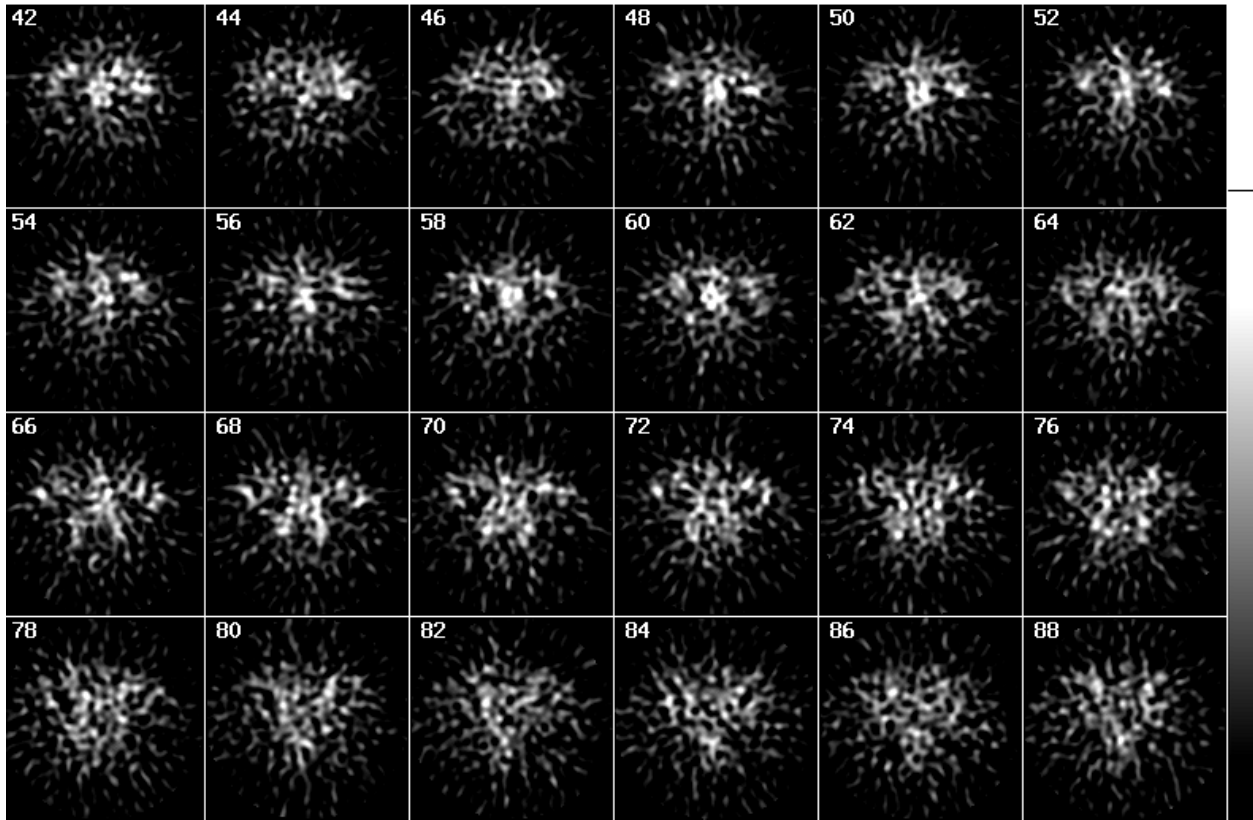
(a)
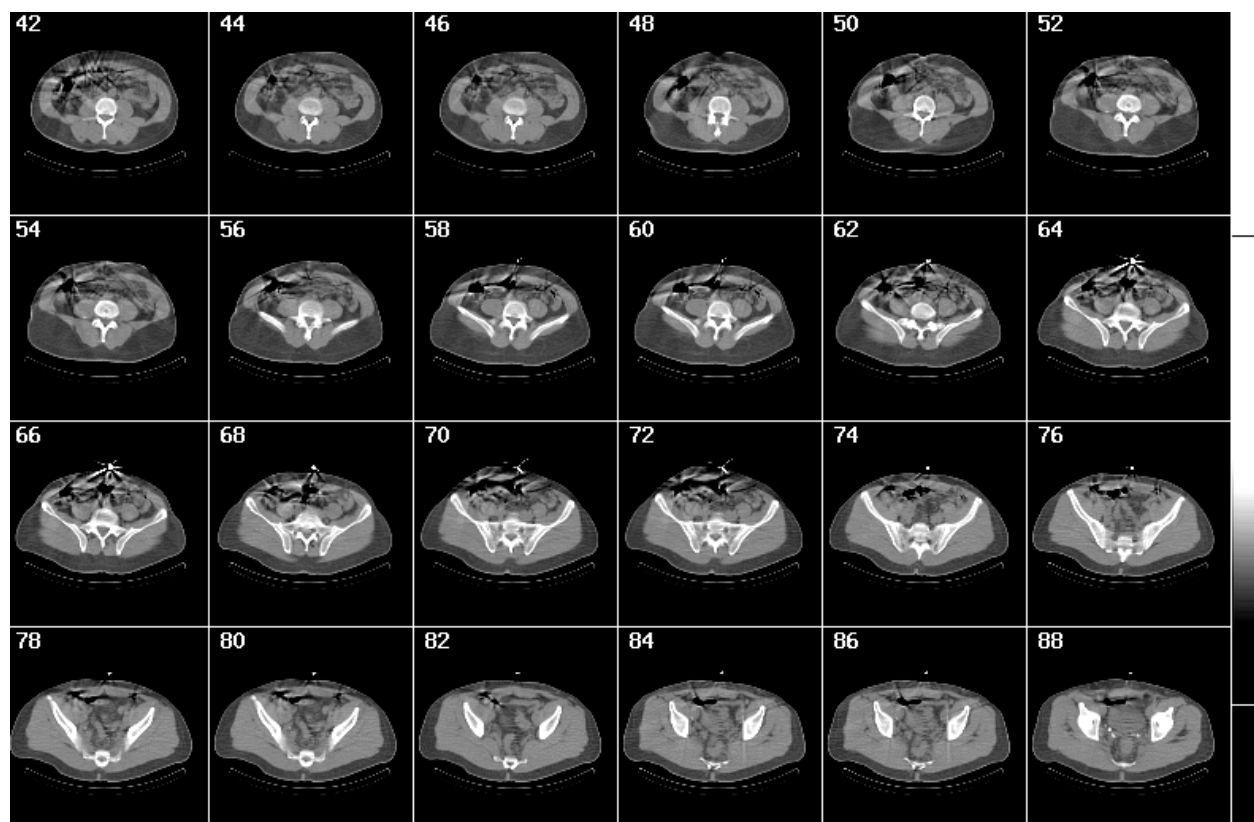
(b)

(c)

(d)

Figure 22. Results from one of the patient ^{111}In PS SPECT studies obtained using a GE VG dual-head SPECT system equipped with a Hawkeye x-ray CT unit. The patient was injected with 5 mCi of ^{111}In PS. The total data acqu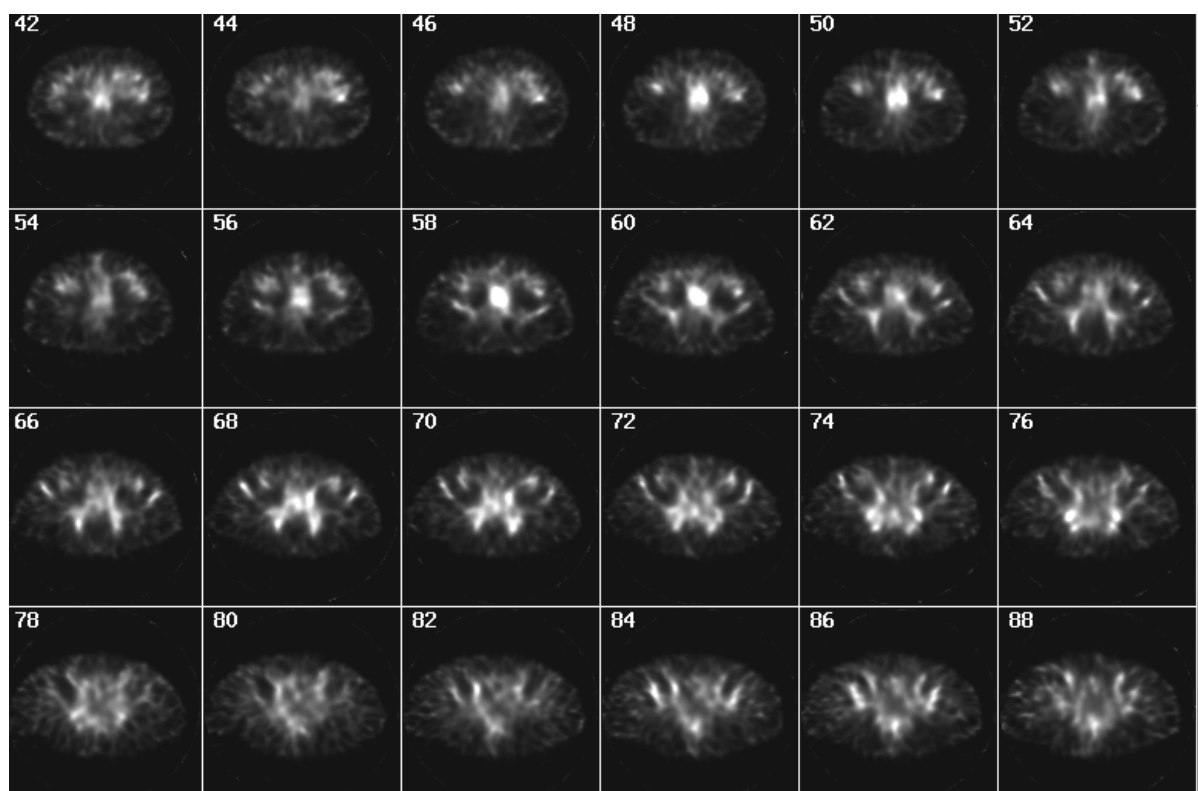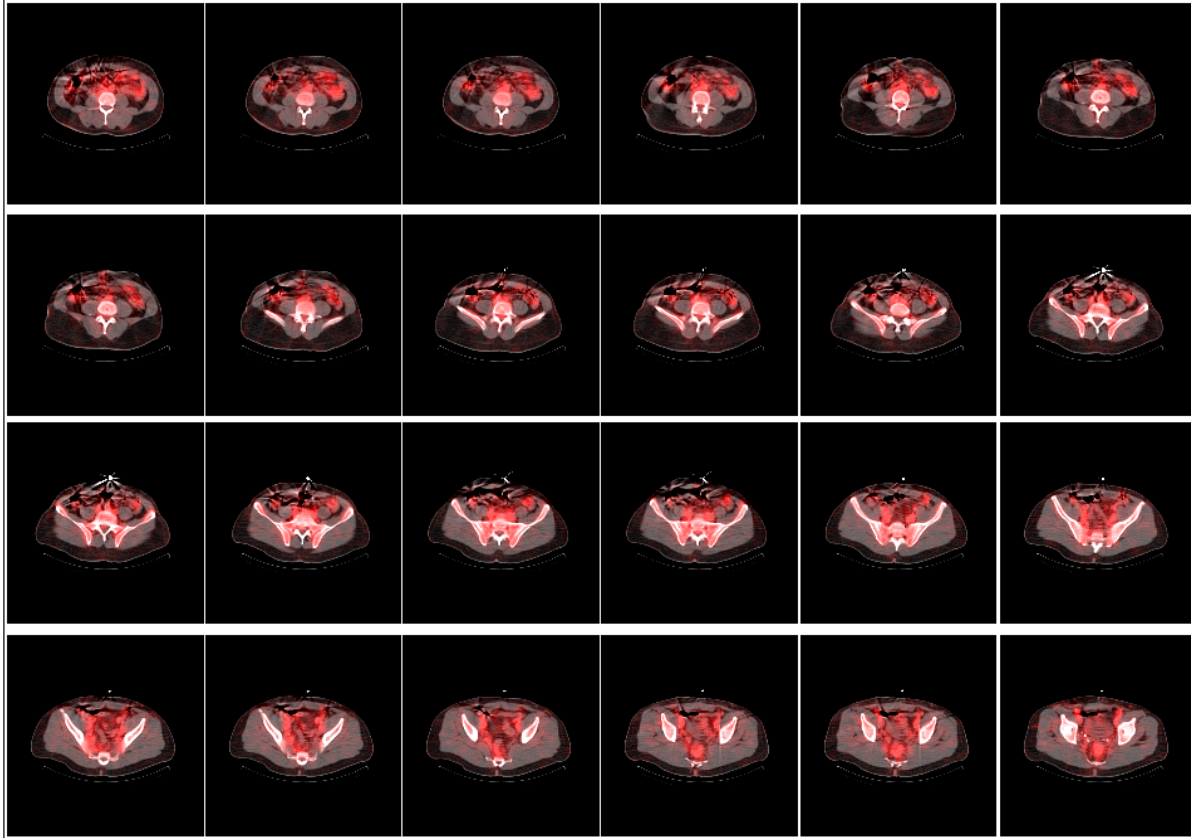isition time was 35 minutes and a GE ME collimator was used. (a) Transaxial reconstructed images obtained using the conventional FBP reconstruction algorithm without any compensation. (b) Corresponding registered transmission CT images from the same patient. (c) Transaxial reconstructed images obtained using the iterative OS-EM algorithm with compensation of photon attenuation and scatter and the full collimator-detector response. Ten subsets and 5 iterations were used in the OS-EM reconstruction. Note the much improved image quality in terms of lower image noise and improved image resolution. (d) Fused SPECT/CT images.

KEY RESEARCH ACCOMPLISHMENTS

1. Completed extension of the realistic 3D NCAT phantom to include the pelvic region of the body. The extended phantom includes the prostate gland, bladder, key blood vessels and major lymph nodes in the pelvic region.

2. Completed the development of a fast simulation method of realistic ^{111}In PS projection data. The method is based on Monte Carlo simulation methods to simulation photon transport inside the phantom and the development of an angular response function (ARF) which accurately models the full imaging characteristics of the collimator-detector response function. The ARF is predetermined using Monte Carlo methods. The fast simulation method is 410 times faster than a straight Monte Carlo simulation method and provides the same accuracy and simulated image quality.

3. Completed the development of corrective image reconstruction methods that incorporate accurate compensation of photon attenuation and scatter in the patient and an accurate model of the full collimator-detector response. It is shown that the corrective image reconstruction methods provide substantial improvement in ^{111}In PS prostate SPECT image quality.

4. Completed the design of the evaluation studies using Hotelling and human observers and to generate data for use in these studies.

5. Completed the creation of a population of 3D NCAT phantoms with variations of anatomy, organ radionuclide uptake distribution, lesion size and location and noise level, to mimic the variations seen in a human population.

6. In the process of generating simulated projection data from the phantom population so as to obtain two classes of images – lesion-present (LP) and lesion-absent (LA) – for use in the CHO study.

7. Work has begun to conduct the evaluation studies to determine the clinical efficacy of the quantitative SPECT image reconstruction methods for ^{111}In PS SPECT imaging of the prostate.

8. Continuing acquisition of patient data and processing using the corrective image reconstruction methods have begun. Twenty-one patient studies have been collected and processed to-date.

REPORTABLE OUTCOMES

Manuscripts
1. Garrity J, Segars WP and Tsui BMW. Development of a Dynamic Model for the Lung Lobes and Airway Tree in the NCAT phantom, in Conference Record of the 2002 IEEE Nuclear Science Symposium and Medical Imaging Conference, Norfolk, VA, November 10-16, 2002.

2. Garrity J, Segars WP and Tsui BMW. Development of a Dynamic Model for the Lung Lobes and Airway Tree in the NCAT phantom. IEEE TNS, 50(3): 378-383, 2003.

3. Sayeram S, Tsui BMW, Zhao XD and Frey EC. Performance Evaluation of 3 Different SPECT Systems Used in In-111 ProstaScint SPECT Imaging. Conference Record of the 2003 IEEE Nuclear Science Symposium and Medical Imaging Conference, October 19-25, 2003, Portland, OR., page 1173, 2004.

4. Frey EC and Tsui BMW. Correction for Collimator Response Function in SPECT. (In) Quantitative Analysis of Nuclear Medicine Images. Kluwer Academic/Plenum Publishers, in press 2005.

5. Tsui BMW and Frey EC. Analytic Image Reconstruction Methods. (In) Quantitative Analysis of Nuclear Medicine Images. Kluwer Academic/Plenum Publishers, 2005.

6. Liu C, Volokh L, Zhao X, Xu Jingyan, Lee TS and Tsui BMW. Performance Evaluation of Block-Iterative Algorithm for SPECT Reconstruction. *Conference Record of the 2005 IEEE Nuclear Science Symposium and Medical Imaging Conference, Puerto, Rico, October 23-29, 2005.*

Presentations
1. Tsui BMW, Zhao XD, Segars WP, Sayeram S and Frey EC. Quantitative In-111 Prostascint SPECT Imaging with Fusion with Anatomical Information. Presented at the 49th Annual Meeting of the Society of Nuclear Medicine, Los Angeles, CA, June 15-19, 2002.

2. Tsui BMW, Du Y, Segars WP, Zhao X and Frey EC. Fast Monte Carlo Simulation Methods for Medium- and High-Energy SPECT. Presented at the 2002 IEEE Nuclear Science Symposium and Medical Imaging Conference, Norfolk, VA, November 10-16, 2002.

3. Sayeram S, Tsui BMW, Zhao XD and Frey EC. Performance Evaluation of three different camera systems Scintillation Crystals used infor 111In-111 Prostascint® SPECT Imaging. Paper presented at the 50th Annual Meeting of the Society of Nuclear Medicine, New Orleans, LA, June 21-25, 2003.

4. Sayeram S, Tsui BMW, Zhao XD and Frey EC. Performance Evaluation of 3 Different SPECT Systems Used in In-111 ProstaScint SPECT Imaging. Paper presented at the 2003 IEEE Nuclear Science Symposium and Medical Imaging Conference, Portland, OR, October 19-25, 2003.

5. Tsui BMW, Zhao X, Frey EC, Shao L, Aarsvold J, Durbin M, Alazraki N and Rollo FD, Evaluation of Quantitative Prostate SPECT/CT using In-111 ProstaScint®. Paper accepted for oral presentation at the 51st Annual Meeting of the Society of Nuclear Medicine, Philadephia, PA, June 19-23, 2004.

6. Tsui BMW, Zhao X, Frey EC, Shao L, Aarsvold J, Durbin M, Alazraki N and Rollo FD, Evaluation of Quantitative Prostate SPECT/CT using In-111 ProstaScint®. Paper presented at the 51st Annual Meeting of the Society of Nuclear Medicine, Philadephia, PA, June 19-23, 2004.

7. Sayeram S., Segars WP and Tsui BMW. Development and Evaluation of Simulated Phantoms for Use in In-111 ProstaScint® SPECT Imaging Studies. Paper to be presented at the 52nd Annual Meeting of the Society of Nuclear Medicine, Toronto, Canada, June 18-22, 2005.

8. Tsui BMW, Chen S, Liu C and Volokh L. Evaluation of Quantitative Image Reconstruction Methods for Maximum Lesion Detectability in In-111 ProstaScint® Prostate SPECT. Paper submitted for the 53rd Annual Meeting of the Society of Nuclear Medicine, San Diego, USA, June 3-7, 2006.

9. Volokh L, Wahl R, Frey EC, Chakraborty D, Du Y, Ziessman H, Zhao X, Jasene H and Tsui BMW. Study of iterative SPECT corrective reconstruction algorithms for lesion detection and localization in In-111 ProstaScint imaging by means of combination of Monte-Carlo simulations and clinical evaluation techniques.

CONCLUSIONS

We have made significance progress in Year 3 of the project. The development of a fast simulation method of realistic ^{111}In PS projection data was completed. The method is based on Monte Carlo simulation methods to simulation photon transport inside the phantom and the development of an angular response function (ARF) which accurately models the full imaging characteristics of the collimator-detector response function and is predetermined using Monte Carlo methods. The fast simulation method is 410 times faster than a straight Monte Carlo simulation method and provide the same accuracy and simulated image quality.

We completed the development of corrective image reconstruction methods that incorporate accurate compensation of photon attenuation and scatter in the patient and an accurate model of the full collimator-detector response. It is shown the corrective image reconstruction methods provide substantial improvement in ^{111}In PS prostate SPECT image quality.

We completed work on generating a population of 3D NCAT phantoms that realistically model the anatomical variations, ^{111}In PS uptake distribution variations and lesion size and location in the patient population. We have started the channelized Hotelling observer experiments and preliminary results have been obtained that indicate the superior quality of the images obtained from the quantitative SPECT image reconstruction methods as compared to the conventional FBP algorithm without any corrections.

We are continuing the acquisition and processing of patient data using the corrective image reconstruction methods. Twenty-one patient studies have been collected to-date.

REFERENCES
1. Greenlee, R.T., et al., *Cancer Statistics.* CA 2000, 2000. **50**: p. 7-33.
2. Moul, J., *Indium-111 capromab pendetide (ProstaScint) for the evaluation of prostate-*

specific antigen-only progression of prostate cancer. New Developments in Prostate Cancer Treatment, 1999. **4**: p. 42-45.

3. Burgers, J.K., G.H. Hinkle, and M.K. Haseman, *Monoclonal antibody imaging of recurrent and metastatic prostate cancer.* Semin Urol, 1995. **13**: p. 103-112.

4. David, V., *MR imaging of the prostate and seminal vesicles.* MRI Clin N Am, 1996. **4**: p. 497-518.

5. Hinkle, G.H., et al., *Multicenter radioimmunoscintigraphic evaluation of patients with prostate carcinoma using Indium-111 capromab pendetide.* Cancer, 1998. **83**: p. 739-747.

6. Kahn, D., et al., *Indium-111 capromab pendetide in the evaluation of patients with residual or recurrent prostate cancer after radical prostatectomy.* J Urol, 1998. **159**: p. 2041-2047.

7. Manyak, M.J., et al., *Immunoscintigraphy with Indium-111 capromab pendetide: Evaluation before definitive therapy in patients with prostate cancer.* Urology, 1999. **54**: p. 1058-1063.

8. Kahn, D., et al., *Radioimmunoscintigraphy with In-111-labeled capromab pendetide predicts prostate cancer response to salvage radiotherapy after failed radical prostatectomy.* J Clin Oncol, 1998. **16**: p. 284-289.

9. Jaszczak, R.J., R.E. Coleman, and C.B. Lim, *SPECT: Single Photon Emission Computed Tomography.* IEEE Trans. Nucl. Sci., 1980. **NS-27**(3): p. 1137-1153.

10. Jaszczak, R.J., C.E. Floyd, Jr., and R.E. Coleman, *Scatter Compensation Techniques For SPECT.* IEEE Trans. Nucl. Sci., 1985. **NS-32**(1): p. 786-793.

11. Jaszczak, R.J., R.E. Coleman, and F.R. Whitehead, *Physical Factors Affecting Quantitative Measurements Using Camera-Based Single Photon Emission Computed Tomography (SPECT).* IEEE Trans. Nucl. Sci., 1981. **NS-28**(1): p. 69-80.

12. Jaszczak, R.J. and B.M.W. Tsui, *Single Photon Emission Computed Tomography (SPECT)*, in *Principles of Nuclear Medicine*, H.N. Wagner, Z. Szabo, and J.W. Buchanan, Editors. 1995, W.B. Saunders: Philadelphia. p. 317-341.

13. Jaszczak, R.J., K.L. Greer, and R.E. Coleman, *SPECT system misalignment: Comparison of phantom and patient images*, in *Emission Computed Tomography*, P. Esser, Editor. 1983, Society of Nuclear Medicine: New York. p. 57-70.

14. Frey, E.C. and B.M.W. Tsui. *A practical method for incorporating scatter in a projector-backprojector for accurate scatter compensation in SPECT*. in *1991 Nuclear Science Symposium and Medical Imaging Conference*. 1991. Santa Fe, NM.

15. Anger, H.O., *Scintillation camera with multichannel collimators.* Journal of Nuclear Medicine, 1964. **5**: p. 515-531.

16. Keller, E.L., *Optimum dimensions of parallel-hole, multiaperture collimators for gamma-ray camera.* Journal of Nuclear Medicine, 1968. **9**: p. 233-235.

17. Metz, C.E., *The geometric transfer function component for scintillation camera collimators with straight parallel holes.* Phys. Med. Biol., 1980. **25**(6): p. 1059-1070.

18. Tsui, B.M.W., et al., *Implementation of simultaneous attenuation and detector response correction in SPECT.* IEEE Transactions on Nuclear Science, 1988. **NS-35**: p. 778-783.

19. Mather, R.L., *Gamma-ray collimator penetration and scattering effects.* Journal Applied Physics, 1957. **28**: p. 1200-1207.

20. Muehllehner, G., *Septal Penetration in Scintillation Camer Collimators.* Phys. Med. Bio., 1973. **18**(6): p. 855-862.

21. DeVries, D.J., *Development and Validation of a Monte Carlo Simulation of Photon Transport in an Anger Camera.* IEEE Trans Med Imag, 1990. **8**(4): p. 430-438.

22. Maniawski, P.J., H.T. Morgan, and F.J.T. Wackers, *Orbit-related variations in spatial*

resolution as a source of artifactual defects in thallium-201 SPECT. Journal of Nuclear Medicine, 1991. **32**: p. 871-875.

23. Shepp, L.A. and Y. Vardi, *Maximum likelihood estimation for emission tomography.* IEEE Transactions on Medical Imaging, 1982. **MI-1**: p. 113-121.

24. Lange, K. and R. Carson, *EM Reconstruction Algorithms for Emission and Transmission Tomography.* J. Comput. Assist. Tomogr., 1984. **8**(2): p. 306-316.

25. Hudson, H.M. and R.S. Larkin, *Accelerated image reconstruction using ordered subsets of projection data.* IEEE Transactions on Medical Imaging, 1994. **13**: p. 601-609.

26. Tsui BMW, Z.X., Wang WT, Tocharoenchai C, Yang Y, Frey EC. *Characterization of Medium and High Energy Collimators for SPECT.* in *Conference Record of the 1999 IEEE Nuclear Science Symposium and the Medical Imaging Conference.* 1999. Seattle, Washington.

27. Tocharoenchai C, T.B., Lewis DP, Frey, E.C., Zhao, XD. *Compensation for the Response Function of a Medium Energy Collimator in Ga-67 Planar and SPECT Imaging.* in *Conference Record of the 1998 IEEE Nuclear Science Symposium and Medical Imaging Conference.* 1998. Toronto, Ontario, Canada: IEEE Press.

28. Lewis, D.P., et al. *Characterization of Medium and High Energy Collimators Using Ray-Tracing and Monte Carlo Methods.* in *Conference Record of the 1998 IEEE Nuclear Science Symposium and the Medical Imaging Conference.* 1998. Toronto, Ontario, Canada: IEEE Press.

29. Tsui BMW, Z.X., Tocharoenchai C, Lewis DP and Frey EC. *Compensation of Collimator Response Function in Quantitative SPECT Using Medium and High Energy Photons.* in *1999 International Meeting on Fully Three-Dimensional Image Reconstruction in Radiology and Nuclear Medicine.* 1999. Egmond Aan Zee, The Netherlands.

30. Tsui BMW, Z.X., Sayeram S, Frey EC, Falen SW and McCartney WH. *Evaluation of Collimator-Detector Response Compensation in Tumor SPECT using Medium and High Energy Collimators.* in *IEEE Medical Imaging Conference and Nuclear Science Symposium.* 2000. Lyon, France: IEEE Press.

31. Barclay, A.B., R.L. Eisner, and E.V. DiBella, *PET Thorax Model Database.* 1996, Crawford Long Hospital of Emory University, Atlanta, GA: http://www.emory.edu/CRL/abb/thoraxmodel.

32. LaCroix, K.J., et al., *Receiver operating characteristic evaluation of iterative reconstruction with attenuation compensation in 99mTc-Sestamibi myocardial SPECT images.* Journal of Nuclear Medicine, 2000. **41**(3): p. 502-513.

33. LaCroix, K.J., *Evaluation of an Attenuation Compensation Method with Respect to Defect Detection in Tc-99m-MIBI Myocardial SPECT Images*, in *Department of Biomedical Engineering.* 1997, The University of North Carolina at Chapel Hill. p. 161.

34. Pretorius, P.H., et al., *Evaluation of right and left ventricular volume and ejection fraction using a mathematical cardiac torso phantom for gated blood pool SPECT.* Journal of Nuclear Medicine, 1997. **38**(10): p. 1528-1534.

35. Pretorius, P.H., et al., *A mathematical model of motion of the heart for use in generating source and attenuation maps for simulating emission imaging.* Medical Physics, 1999. **26**(11): p. 2323-2332.

36. Segars, W.P., D.S. Lalush, and T. BMW, *A realistic spline-based dynamic heart phantom.* IEEE Trans Nucl Sci., 1999. **46**(3): p. 503-506.

37. Segars, W.P., D.S. Lalush, and T. BMW, *Modeling Respiratory Mechanics in the MCAT and*

Spline-Based MCAT Phantoms. IEEE Trans Nucl Sci., 2001.

38. Segars, W.P., D.S. Lalush, and B.M.W. Tsui. *Modeling Respiratory Mechanics in the MCAT and Spline-Based MCAT Phantoms.* in *Conference Record of the 1999 IEEE Nuclear Science Symposium and the Medical Imaging Conference.* 1999. Seattle, Washington: IEEE Press.

39. de Vries, D.J., et al., *Evaluation of the effect of scatter correction on lesion detection in hepatic SPECT imaging.* Ieee Transactions On Nuclear Science, 1997. **44**(5): p. 1733-1740.

40. de Vries, D.J., et al., *Effects of scatter subtraction on detection and quantitation in hepatic SPECT.* Journal of Nuclear Medicine, 1999. **40**(6): p. 1011-1023.

41. Wollenweber, S.D., Tsui BMW, Lalush DS, Frey ED, Lacroix KJ, Gullberg GT. *Comparison of Radially-Symmetric Versus Oriented Channel Models using Channelized Hotelling Observers for Myocardial Defect Detection in Parallel-Hole SPECT.* in *Conference Record of the 1998 IEEE Nuclear Science Symposium and the Medical Imaging Conference.* 1998. Toronto, Ontario, Canada: IEEE Press.

42. LaCroix, K.J., B.M.W. Tsui, and E.C. Frey. *Oriented vs. Non-oriented Frequency Channels for the Hotelling Observer: A Comparison with Human Observers.* in *Conference Record of the 1999 Nuclear Science Symposium and the Medical Imaging Conference.* 1999. Seattle, Washington.

43. Frey, E.C., K.J. LaCroix, and T. BMW, *Application of Detection Task Based Measures of Image Quality to Optimization and Evaluation of Three-Dimensional Reconstruction-Based Compensation Methods in Myocardial Perfusion SPECT.* IEEE Trans Med Imaging.

44. Wollenweber, S.D., et al. *Evaluation of Myocardial Defect Detection between Parallel-hole and Fan-beam SPECT using the Hotelling Trace.* in *Conference Record of the 1997 IEEE Nuclear Science Symposium and Medical Imaging Conference.* 1997. Albuquerque, NM.

45. Wollenweber, S.D., et al., *Evaluation of myocardial defect detection between parallel-hole and fan beam SPECT using Hotelling Trace.* IEEE Transactions on Nuclear Science, 1998. **45**: p. 2205-2210.

46. Achtert, A.-D., et al., *An investigation of the estimation of EF and cardiac volumes by a quantitative gated SPECT software package in simulated gated SPECT perfusion images.* J Nucl Cardiol, 1998. **5**(2): p. 144-152.

47. Kadrmas, D.J., *Simultaneous technesium-99m/Thallium-201 SPECT imaging with model-based compensation for cross-contaminating effects.* Physics in Medicine and Biology, 1999. **44**: p. 1843-1860.

48. Swenson, R.G., *Unified measurement of observer performance in detecting and localizing targe objects on images.* Medical Physics, 1996. **23**: p. 1709-1725.